Diffraction imaging point of common-offset gather: GPR data example

J.J.S. de Figueiredo (DEP/UNICAMP, Brazil), F. Oliveira (CPGF/UFPA and FACEN/UFPA, Brazil), E. Esmi (IMECC/UNICAMP, Brazil), L. Freitas (Geoprocessados, Mexico), S. Green (University of Houston), A. Novais and J. Schleicher (IMECC/UNICAMP and INCT-GP, Brazil)*

SUMMARY

Hydrocarbon traps are generally located beneath complex geological structures. Such areas contain many seismic diffractors that carry detailed structure information in the order of the seismic wavelength. Therefore, the development of computational resources capable of detecting diffractor points with a good resolution is desirable, but has been a challenge in the area of seismic processing. In this work, we present a method for the detection of diffractor points in the common-offset gathers domain. In our approach, the diffraction imaging is based on the diffraction operator, which can be used in both the time and depth domains, in accordance with the complexity of the area. This method, which does not require any knowledge apart from the migration velocity field (i.e., rms velocities or interval velocities) applies pattern recognition to the amplitudes along the diffraction operator. Numerical examples using synthetic and real data demonstrate the feasibility of the technique.

INTRODUCTION

It is well known that hydrocarbon reservoirs commonly are located in geological stsructures that are difficult to image with seismic methods and obtain high resolution. This structures include common hydrocarbon traps, such as faults, pinch-outs, unconformities, salts domes, and other structures the size of which is of the order of the wavelength (Trorey, 1970).

Because of the importance of these types of structures, several methods for imaging diffractions have been developed in the recent past. The first authors to look into the topic were Landa et al. (1987) and Landa and Keydar (1998), who proposed and refined a detection method related to specific kinematic and dynamic properties of diffracted waves. Another approach (Moser and Howard, 2008) is based on suppressing specular reflections to image diffractions in the depth domain. Most recently, Zhu and Wu (2010) developed a method based on the local image matrix (LIM), which uses an image condition in the local incident and reflection angles for source-receiver pairs to detect diffractions.

In this work, we propose a diffraction detection method based on an amplitude analysis along the elementary diffractions (Tabti et al., 2004). This method does not require any knowledge apart of from the migration velocity field, i.e., rms velocities or interval velocities depending on the complexity of the area. It applies pattern recognition to the amplitudes along the diffraction operator. Numerical examples on synthetic and ground penetrating radar (GPR) field data demonstrate the feasibility of the method.

METHOD

Diffraction operator

Tabti et al. (2004) introduced amplitude analysis along elementary diffractions for Fresnel aperture specification. As illustrated in Figure 1a, the traveltime of an elementary diffraction associated with a reflection point is tangent to the reflection traveltime at the stationary point (location of the specular reflection event). More specifically, in limited bandwidth situations, this tangential point becomes a tangential contact region, which defines the minimum aperture for true-amplitude Kirchhoff migration (Schleicher et al., 1997). (Tabti et al., 2004) named it the Fresnel aperture due to its close relationship to the Fresnel zone. For image point off any reflectors or diffractors, below referred to as "void image points", there is no such region. The traveltime of the elementary diffraction associated with a void image point may cross some reflection events, but won't be tangential to any events (see Figure 1b), except for extremely rare coincidental situations.

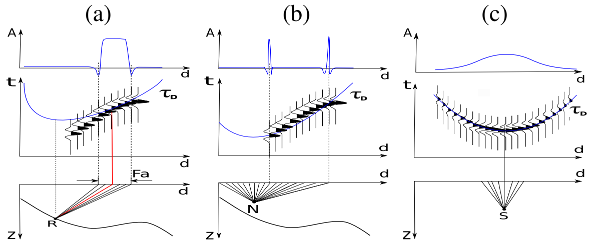

Figure 1: (Illustration of the diffraction operator for (a) a reflection point and (b) a void image point. Top: amplitude along the diffraction operator; center: diffraction traveltime and seismic event; bottom: image point and ray family. (c) Illustration of the diffraction operator for a diffraction point. Top: amplitude along the diffraction operator; center: diffraction traveltime and seismic event; bottom: image point and ray family.

Tabti et al. (2004) described amplitude analysis along elementary diffractions by means of a diffraction operator D. This operator derives from the Kirchhoff depth migration integral (Schleicher et al., 1993)

$$I(M) = \int_{A_f} d^2\xi \, W(M,\xi)\partial_t U(\xi,t)|_{t=\tau_D(M,\xi)} \qquad (1)$$

where $U(\xi,t)$ is the seismic data measured at ξ, $\tau_D(M,\xi)$ is the traveltime of the elementary diffraction of M, A_f is the Fresnel aperture, and $W(M,\xi)$ is a weight function. For simplicity, we omit the weight function in the present study, i.e. $W(M,\xi) = 1$. Integration variable ξ is the horizontal coordinate of the seismic section to be migrated, for instance the midpoint coordinate for a common-offset section or the receiver coordinate for a common-shot section.

Instead of performing the summation, the diffraction operator $D(M)$ at an image point M collects a single valued curve (or surface, in the 3D case), defined as a function of the integration variable ξ. Its value at ξ is the amplitude the stack in equation 1 will consider at ξ. This value defines the amplitude of the elementary diffraction measured at ξ. More specifically,

$$D(M,\xi) = W(M,\xi)\partial_t U(\xi,t)|_{t=\tau_D(M,\xi)} . \qquad (2)$$

In this paper, we restrict ourselves to a simplified version of the diffractor operator proposed by Tabti et al. (2004), based on the Kirchoff time migration integral for common-offset configuration. Therefore, the elementary diffraction traveltime $\tau_D(M,\xi)$ is given by (Landa et al., 1987)

$$\tau_D(M,\xi) = \sqrt{(\frac{t_0}{2})^2 + (\frac{\xi - h}{2})^2} + \sqrt{(\frac{t_0}{2})^2 + (\frac{\xi + h}{2})^2} \quad (3)$$

where t_0 is zero-offset time for any point at subsurface, h is the half-offset and v is medium velocity.

Tabti et al. (2004) also noted that in the case of a diffractor point (either a point scatterer or an edge), the corresponding elementary diffraction corresponds to the scattered seismic event. The Fresnel aperture then extends theoretically to infinity, regardless of the frequency content of the source pulse. Figure 1(c) illustrates the diffraction operator at a diffraction point.

Figures 1 form the basis of our diffraction imaging algorithm explained in the next section. The main idea of our detection method is to classify every point in the image domain M as a diffractor, reflector or noise point by means of the characteristics of its diffraction operator $D(M,\xi)$. The approach consists in straightforward classification using a well-established pattern-recognition technique called k-nearest-neighbors (kNN).

Diffraction imaging by pattern recognition

Pattern recognition aims at classifying data (patterns) based either on a priori knowledge or on statistical information extracted from the patterns (Duda and Hart, 1973; Theodoridis and Koutroumbas, 1999). Pattern recognition techniques have found applications in various areas, for instance, decision making, inspection of objects, and automatic character recognition (Theodoridis and Koutroumbas, 1999).

The mathematical tool to achieve this aim is called a classifier. Suppose we are faced with the problem to classify a certain set of patterns into N classes, $w_1,\cdots,w_n$. Let $x_1,\cdots,x_p \in I\!R^n$ be samples of patterns whose class is already known, and $C_i \subseteq \{x_1,\cdots,x_p\}$ be a subset of patterns associated with class w_i such that $C_j \cap C_i = \emptyset$ for $i \neq j$, i.e., there are no subsets that fall into two different classes at the same time. Given an arbitrary pattern x, a classifier aims at associating x with one of the N classes. In this work, we are only concerned in imaging diffractions. Therefore we use two classes ($N = 2$): the diffraction class C_0 and the non-diffraction class C_1 (that includes both noise and reflection image points). We also restrict ourselves to the so-called k-nearest-neighbour (kNN) classifier, because of its simple implementation.

The kNN classifier is a supervised method to solve problems in pattern recognition. It is a method for classifying objects based on a certain distance measure and a fixed set of samples in the feature space for which the associated label of class is already known. The development of the kNN classifier was inspired by the technique for the estimation of a non-parametric probability density function (PDF) called k-nearest-neighbour density estimation, which is basically a variation of the histogram approximation of an unknown PDF. Moreover, although no assumptions about PDFs need to be made, the strategy used by the kNN model to classify patterns reminds of the well-known Bayes classification rule (Duda and Hart, 1973; Theodoridis and Koutroumbas, 1999).

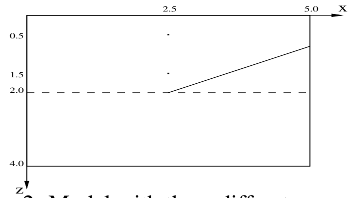

Figure 2: Model with three diffractors.

Let $k \leq p$ be a positive fixed integer and $dist$ a distance measure in $I\!R^n$. Then, the kNN classification process is given by the following rules (Theodoridis and Koutroumbas, 1999)

- Find the k nearest neighbours of x in the set $\{x_1,\cdots,x_p\}$ in terms of their distances $dist(x,x_i)$, for $i = 1,\cdots,p$. Let the symbols $\tilde{x}_1,\cdots,\tilde{x}_k \in \{x_1,\cdots,x_p\}$, with $\tilde{x}_i \neq \tilde{x}_j$ for $i \neq j$, denote those k nearest neighbours.
- Identify the number k_i of patterns $\tilde{x}_i$ among these k nearest neighbours that belong to class w_i for $i = 1,\cdots,N$.
- Assign x to the class w_j with the maximum number k_j of samples.

Since the results of a kNN model depend of choice of the number k of nearest neighbours, techniques to select an appropriate parameter k like, for example, cross-validation, can be employed. Also, the performance may vary as a function of the distance measure considered. Usually, Euclidean distance is used as the distance metric.

As with all supervised models, the accuracy of the kNN classifier depends on the given training set. If non-representative samples of classes are used as training data, the performance of kNN classification can be severely degraded.

In the simulations described in the Numerical Examples section, we have employed a value of $k = 1$ and the Euclidean distance measure.

RESULTS AND DISCUSSION

Synthetic example I: Model with three diffractors

The first model consists of two diffraction points and one dipping reflector with an endpoint in the center of the model, buried in a constant-velocity background with $v = 2000$ m/s (see Figure 2).

The synthetic dataset was generated by Kirchhoff modelling. It simulates a zero-offset section with 500 source-receivers pairs spaced at 10 m covering an extension of 5000 m. To the synthetic data we added random noise with a signal-to-noise ratio (S/N) of 100 with respect to the reflection event, which corresponds to a S/N of about 10 for the diffraction events (see Figure 3).

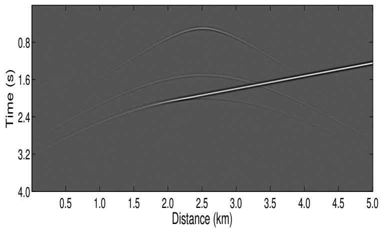

Figure 3: Zero-offset dataset obtained by Kirchhoff modeling.

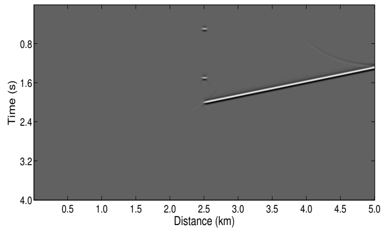

Figure 4: Time-migrated image of dataset from Figure 3.

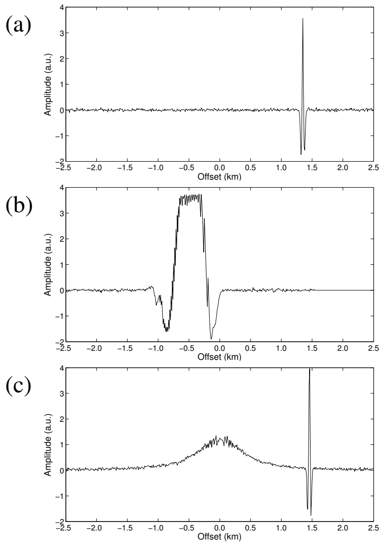

Figure 5: Diffraction operators of image locations in Figure 4 associated to (a) a void ($x = 2.5$ km, $t = 0.8$ s), (b) a reflection ($x = 3.5$ km, $t = 1.73$ s) and (c) a diffraction ($x = 2.5$ km, $t = 0.5$ s) point.

Conventional Kirchhoff migration of these data produces the image shown in Figure 4. While this image contains all three diffraction points, the two isolated diffraction points have rather low amplitudes and would be hard to visualize in noisy data. Only the endpoint of the reflector is clearly identifiable as a diffraction point. Figure 5 shows the diffraction operators of image locations associated to (a) a void ($x = 2.5$ km, $t = 0.8$ s), (b) a reflection ($x = 3.5$ km, $t = 1.73$ s) and (c) a diffraction ($x = 2.5$ km, $t = 0.5$ s) point, respectively.

As suggested by Landa et al. (1987), we normalized the dataset trace-by-trace using its envelope (Figure 6). Figure 7 shows the diffraction panels for the profile located at $x = 2.5$ km obtained from the raw data Figure 7a and from the normalized data Figure 7b. The diffraction amplitudes (flat events) are equalized to the reflections (other events).

For this case, we started by devising a kNN classifier using only two classes ($N = 2$): the diffraction class C_0 and the non-

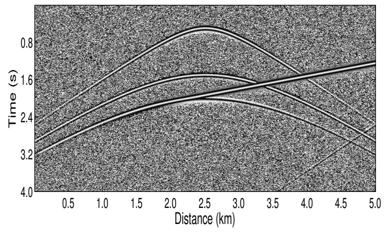

Figure 6: Normalized dataset.

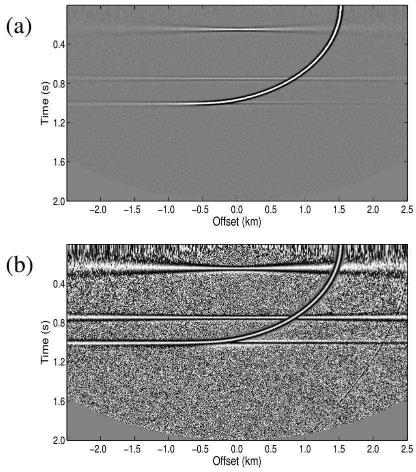

Figure 7: Diffraction panels at 2.5 km obtained from the (a) raw data and (b) normalized data.

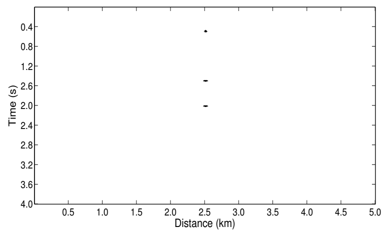

Figure 8: Image points classified as belonging to the diffraction class by the kNN classifier.

diffraction class C_1 (that includes both reflection and void image points). To train the kNN classifier, we used the diffraction operators evaluated at the two isolated point diffractors as training patterns for the diffraction class. The training patterns for the non-diffraction class were the diffraction operator at several locations, including reflector and void image points. We then applied the so-trained kNN classifier to the diffraction operators of the whole normalized dataset. The result is depicted in Figure 8.

We see that the method has correctly identified and positioned all three diffractor points in the model, i.e., the two isolated point diffractors used for the training and also the tip of the reflector not used in the training process. Moreover, it has not misidentified any additional points as diffractions.

Real data example: Ground Penetrating Radar dataset

For a more meaningful test, we applied this method to GPR data. The data set is from a survey conducted over four metal drain pipes crossing under a road at the University of Houston Coastal Center, located in La Marque, Texas, United States

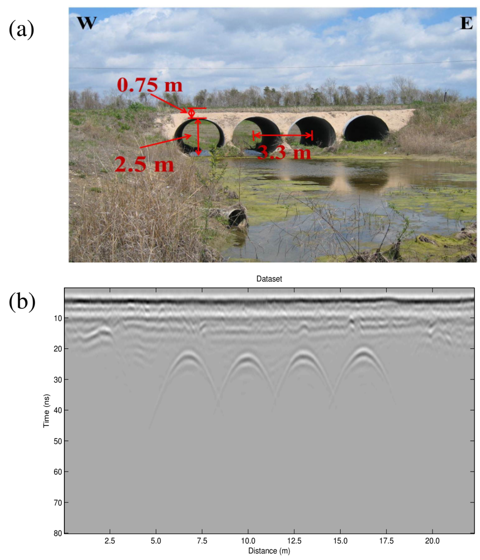

Figure 9: (a) Metal pipes located in La Marque, Houston, Texas, United States. (b) 250 MHz GPR profile showing diffractions from the pipes.

(Figure 9a). Since the survey line was perpendicular to the direction of the pipes, prominent diffractions from the pipes occur. Because of the high reflectivity and attenuation of metal, GPR reflections from the pipes occur only from the exterior of the pipes and not from inside de pipes (Zeng and McMechan, 1997). Figure 9b shows the 250 MHz GPR profile acquired. The distance between the transmitter and reciever antennas was 0.28 m (half-offset 0.14 m), and the interval between traces was 0.05 m A total of 445 traces were collected along the 22.25 m survey line. The length of the time window was 99 ns and the number of samples per trace was 247, resulting in a time sampling rate of 0.4 ns.

Figure 10a shows the profile of Figure 9b after normalization, and Figure 10b shows the diffraction panel for the profile located at $x = 10$m obtained from the normalized data.

The Kirchhoff time-migrated section of the GPR data is shown in Figure 11a. The velocity used for migration was 0.088 m/ns ($0.88x10^8$ m/s). This velocity collapsed all diffractions and is within the expected range for soil mixtures. Figure 11b shows the result of the diffraction imaging approach using pattern recognition with the kNN classifier algorithm trained on the synthetic data as detailed above.

As we can see in this figure, the kNN classifier was successfully applied to the real field data from GPR. Comparing the section migrated (see Figure 11a) with section classified (see Figure 11b) we can see that the kNN classifier did not produce any false positives and that all four diffractions were clearly identified.

CONCLUSIONS

In this work, we used the diffractor operator proposed by Tabti et al. (2004) as a tool for diffraction imaging. It consists of a straightforward application of a pattern recognition technique to identify and distinguish diffraction events from reflection events and noise areas by their amplitude pattern. In our

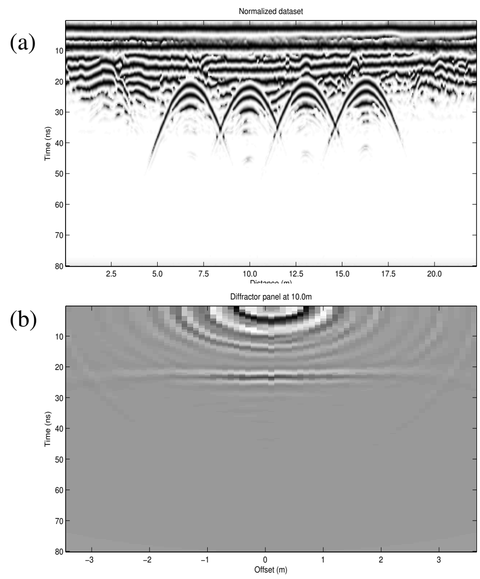

Figure 10: (a) GPR data normalized. (b) The diffraction panel for the profile located at x = 10 m.

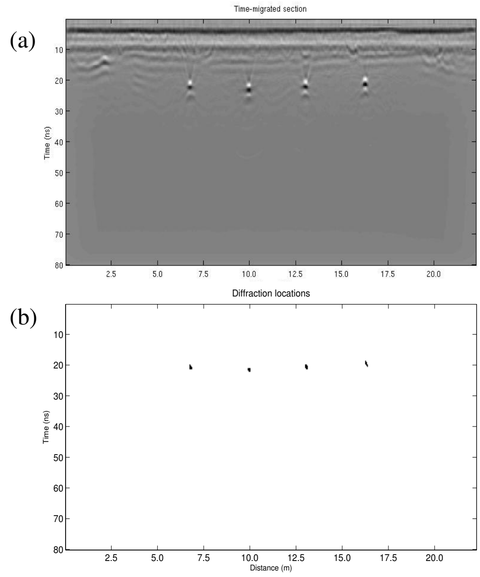

Figure 11: (a) Time-migration profile. (b) Four diffraction locations identified by kNN classifier.

numerical experiments, the approach based on the k-nearest-neighbours (kNN) classifier showed promising results. After training with selected diffraction operators pertaining to a synthetic data set from a very simple synthetic model, the kNN classifier was able to correctly detect all diffraction points not only in a complicated synthetic data sets, but also in a real GPR dataset, not missing a single point and not creating a single false positive.

ACKNOWLEDGEMENTS

The authors wish to thank CAPES, CNPq, and FAPESP, as well as Petrobras and the sponsors of the WIT consortium for financial support. We grateful to the Allied Geophysical Laboratories team for the GPR data.

EDITED REFERENCES

Note: This reference list is a copy-edited version of the reference list submitted by the author. Reference lists for the 2011 SEG Technical Program Expanded Abstracts have been copy edited so that references provided with the online metadata for each paper will achieve a high degree of linking to cited sources that appear on the Web.

REFERENCES

Duda, R., and P. Hart, 1973, Pattern classification and scene analysis: John Wiley & Sons.

Landa, E., and S. Keydar, 1998, Seismic monitoring of diffraction images for detection of local heterogeneities: Geophysics, **63**, no. 3, 1093–1100, doi:10.1190/1.1444387.

Landa, E., V. Shtivelman, and B. Gelchinsky, 1987, A method for detection of diffracted waves on commom-offset sections: Geophysical Prospecting, **35**, no. 4, 359–373, doi:10.1111/j.1365-2478.1987.tb00823.x.

Moser, T., and C. Howard, 2008, Diffraction imagining in the depth: Geophysical Prospecting, **56**, no. 5, 627–641, doi:10.1111/j.1365-2478.2007.00718.x.

Schleicher, J., P. Hubral, M. Tygel, and M. S. Jaya, 1997, Minimum apertures and Fresnel zones in migration and demigration: Geophysics, **62**, no. 1, 183–194, doi:10.1190/1.1444118.

Schleicher, J., M. Tygel, and P. Hubral, 1993, 3-D true- amplitude finite-offset migration: Geophysics, **58**, no. 8, 1112–1126, doi:10.1190/1.1443495.

Tabti, H., J. Gelius, and T. Hellmann, 2004, First break: Fresnel aperture prestack depth migration, **22,** 39–46.

Theodoridis, S., and K. Koutroumbas, 1999, Pattern recognition: Academic Press.

Trorey, A. W., 1970, A simple theory for seismic diffractions: Geophysics, **35**, no. 5, 762–784, doi:10.1190/1.1440129.

Zeng, X., and G. A. McMechan, 1997, GPR characterization of buried tanks and pipes: Geophysics, **62**, no. 3, 797–806, doi:10.1190/1.1444189.

Zhu, X., and R. Wu, 2010, Imaging diffraction points using the local image matrices generated in prestack migration: Geophysics, **75**, no. 1, S1–S9, doi:10.1190/1.3277252.